

RSC Advances



This is an *Accepted Manuscript*, which has been through the Royal Society of Chemistry peer review process and has been accepted for publication.

Accepted Manuscripts are published online shortly after acceptance, before technical editing, formatting and proof reading. Using this free service, authors can make their results available to the community, in citable form, before we publish the edited article. This *Accepted Manuscript* will be replaced by the edited, formatted and paginated article as soon as this is available.

You can find more information about *Accepted Manuscripts* in the [Information for Authors](#).

Please note that technical editing may introduce minor changes to the text and/or graphics, which may alter content. The journal's standard [Terms & Conditions](#) and the [Ethical guidelines](#) still apply. In no event shall the Royal Society of Chemistry be held responsible for any errors or omissions in this *Accepted Manuscript* or any consequences arising from the use of any information it contains.

ARTICLE TYPE

Cite this: DOI: 10.1039/c0xx00000x

www.rsc.org/xxxxxx

Filled and peptide-modified single-walled carbon nanotubes: synthesis, characterization, and in vitro test for cancer cell targetingZhiyuan Hu^{1,2*} Zhaozheng Song¹ and Chunpeng Yang¹

Received (in XXX, XXX) Xth XXXXXXXXX 20XX, Accepted Xth XXXXXXXXX 20XX

DOI: 10.1039/b000000x

Abstract: Multi-functional single-walled carbon nanotubes (SWNTs) with metal endohedral filling and a high degree of polycarboxylation on the sidewalls were synthesized without affecting the SWNT σ -framework. The encapsulation of Zr^{4+} ions within SWNTs from aqueous solutions by the wet chemistry method was achieved using tubes “corked” with C_{70} at both ends to prevent the loss of the loaded metal. Carboxylic acid functionalities were introduced on the sidewalls of the tubes without introducing holes in the framework through a modified Birch-type reaction. Moreover, these metal-filled, surface polycarboxylated SWNTs can serve as versatile anchor points for coupling to specific peptides, which can target integrins for potential applications in diagnostic imaging and therapy. This directly leads to the construction of multi-functional SWNT conjugates, equipped with peptides on the surface for the targeting delivery of radionuclides to specific sites in-vivo. The different SWNT adducts were characterized by Raman spectroscopy, ultraviolet-visible/near-infrared (UV-vis/NIR) spectroscopy, thermogravimetric analysis combined with mass spectrometry and also transmission electron microscopy (TEM). The aqueous solubility, cytotoxicity and cancer cells binding assay were studied for investigation the potentiality of these multi-functional SWNT conjugates in biomedical application.

1. Introduction

Since the discovery of carbon nanotubes (CNT) by Iijima,¹ many scientists from different groups all over the world have been attracted to these materials and a large number of studies have been carried out to promote potential applications in electricity, advanced materials, and medicine. However, the low solubility and rapid formation of bundles when dispersed in most common solvents have proved to be obstacles in the advancement of industrial applications. Normally, the direct method for increasing the CNTs' solubility is the introduction of carboxylic groups (-COOH) on the surface of the nanotube scaffold via oxidation. The most important factor of this modification is that some subsequent functionalities including polymers or biomolecules can be anchored on the nanotube surface via coupling through the carboxylic group.²⁻⁷ The issue with this method is that the σ bonds in the nanotube structure need to be broken for the subsequent oxidation reaction. This means that the nanotube structure is inevitably damaged by the introduction of holes on the surface during oxidation. As such, the unique properties and electronic network of the tubes are affected. Some

non-covalent wrapping methods based on *van der Waals* forces and aromatic stacking have been reported for the modification of CNTs without affecting the characteristic of tubes.^{8,9}

An electrophilic addition of CO_2 to reduced nanotubes by Birch reduction is a selective and efficient method for the introduction of carboxylic acid functionalities without affecting the single-walled carbon nanotube (SWNT) σ -framework.¹⁰ The direct electrophilic addition of CO_2 to the SWNT sidewalls without breaking σ bonds can maintain the structure of the nanotube scaffold. This approach can also achieve a very high degree of functionalization because CNTs are reduced to negatively charged intermediates (CNT^{-1}) in liquid ammonia by lithium metal¹¹⁻¹³ prior to the addition of CO_2 . This degree of functionalization tunable by varying different reaction conditions (reaction time, ultrasonic treatment and pressure).

If the nanotube structure is kept intact without introducing holes on the sidewall, endohedral filling of the surface functionalized SWNTs with some metals will build a complex construct with interior filling and functionalities on the sidewall simultaneously. High-yield filling of SWNTs with different kinds of halides including $ThCl_4$,¹⁴ $CdCl_2$,¹⁴ $TbCl_3$, $TiCl_4$, and PbI_2 , lanthanide halides $LnCl_3$,¹⁵ KI ,^{16, 17} $ZrCl_4$,¹⁸ and silver halides

under harsh conditions (above 300 °C) leading to continuous crystalline filling was demonstrated by Professor Malcolm L.H. Green's group at Oxford. In this typical endohedral filling method via a molten salt route, the end of the nanotubes normally close under the reaction conditions, which involves the thermal annealing of the SWNTs under harsh conditions, *e.g.*, samples are heated at temperatures at least 20 °C above the melting point of the filling material.¹⁹ The condition of this typical endohedral filling method via a molten salt route is very harsh (above 300 °C) and time-consuming (about 24 h). Considering the practical constraints of typical chemistry laboratories, in our experience the molten salt route is not compatible with the rapid generation of metal filling carbon nanotubes in aqueous media for the further radiochemistry. Therefore we developed and report here a new protocol for the rapid metal filling under mild conditions in aqueous media, which can be generalised to be applicable to water soluble radionuclide precursors in the future. A stopper molecule with a compatible outer diameter (C₇₀) is encapsulated within the inner cavity of the tubes simultaneously with the metal to minimise the leaking of the payload in aqueous media.

In recent decades, synthetic peptide-based targeting fluorescence/PET probes have been developed for diagnostic imaging and therapy. This is because of their advantages compared with large-sized antibodies: specific peptides are easily synthesized and modified, and they are less likely to be immunogenic and have rapid blood clearance.²⁰⁻²⁴ The gastrin-releasing peptide receptor (GRP-R) targeting peptide such as Bombesin is very good candidate for visualizing tumors earlier in diagnosis, such as prostate, non-small cell lung carcinoma, breast, and gastrointestinal stromal tumors.²⁵ Tumor progression, invasion, and metastasis of breast cancer, glioma, melanoma, and ovarian carcinoma are linked to a specific biomolecule $\alpha_v\beta_3$ integrin over-expression during tumor angiogenesis. Pentapeptide cyclo(-Arg-Gly-Asp-DPhe-Val-) was developed by Kessler and co-workers and showed high affinity and selectivity for $\alpha_v\beta_3$ integrin.²⁶⁻²⁸ Moreover, cyclo-(RGDFK) is one the most prominent structures for the development of molecular imaging agents for the assessment of $\alpha_v\beta_3$ expression.

The aim of this study was to build a complex construct with a receptor targeting peptide anchored on the surface of polycarboxylate-functionalized SWNTs and potential radionuclide metals in the interior of nanotube scaffold. SWNTs used here were purified by the "steam" method with open ends, clean surface first. Metal filling in the hollow cavity of the SWNTs was achieved by the aqueous method under mild conditions. C₇₀ was encapsulated within the inner cavity of the tubes to prevent load loss. A modified Birch-type reaction was explored in order to extend a type selective polycarboxylation of endohedral filled CNTs via gaseous carbon dioxide. After constructing endohedral filled SWNTs-COOH_x complexes, the entire surface of the CNTs were rendered biocompatible *via* covalent functionalization with two cancer-targeting peptides (RGDFK and Bombesin).

2 Materials and methods

2.1 Filling carbon nanotubes with Zirconium Acetate Zr(OAc)₄

Open-ended and steaming purified (see supporting material)

SWNTs (1.6 mg) were added to 20 mL of ethanol and then ultrasonicated in a water bath for 20 min. SWNTs ethanol solution was splitted into two samples (A and B). 23.4 mL of zirconium acetate solution (30 mg) was added to each vial. 10 mg of sodium acetate was added into B sample. Zr(OAc)₄ formed gel in both samples after two days room temperature stirring. H₂SO₄ was added into both samples in dropwise until the pH value was adjusted to 2.4 for avoiding the gel formation of Zr(OAc)₄. Ethanol was removed by evaporation and then 10-15 mL double-distilled H₂O was added into each sample without the gel forming by dropping H₂SO₄. Samples were kept under constant stirring at 50 °C for 48 h. The solution was filtered through a 0.2 μm polycarbonate membrane and washed with excess distilled water to remove the large excess of Zr(OAc)₄ and sodium acetate. The sample was then dried under vacuum giving zirconium acetate filled SWNTs, designated as Zr(OAc)₄@SWNTs. Also the unwashed Zr(OAc)₄@SWNTs solution can be "corked" with C₇₀. Prior to washing, C₇₀ (0.4 mg) was added, stirred and heated at 50 °C overnight. After 24 h, the solution was filtered and washed several times with excess double-distilled H₂O, followed by toluene wash to remove the C₇₀ left in solution and attached the sidewall of SWNTs.

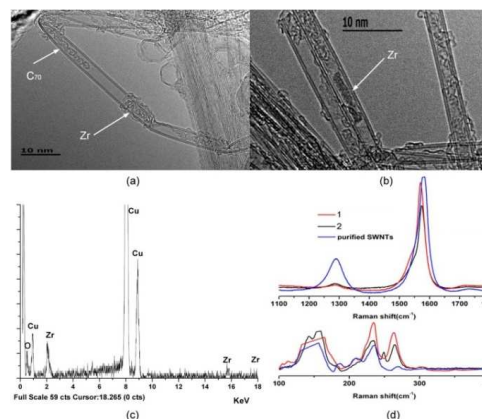


Figure 1. Typical HRTEM images of (a) C₇₀@Zr⁴⁺@SWNTs(1) observed in Zr-filled and C₇₀ corked samples. (b) HRTEM of Zr⁴⁺ encapsulated inside steam purified SWNTs. (c) The EDS spectrum of C₇₀@Zr⁴⁺@SWNTs(1). (d) Solid state Raman spectrum of C₇₀@Zr⁴⁺@SWNT (1, 2) when filling was achieved in the presence or absence of NaOAc ($\lambda_{\text{exc}}=830$ nm) showing the intensity of G and D bands vs Raman shift (cm⁻¹) (up) RBM frequency modes (bottom).

2.3 Reductive polycarboxylation functionalization of SWNTs

Steam purified SWNTs (20 mg, 1.66 mmol of carbon) were dispersed in 200 mL DMSO after 30 min ultrasonication in a heat-dried and argon purged under 30 min ultrasonication four-necked round-bottom flask (500 mL) equipped with two gas inlets and pressure compensation. The dispersion was cooled to -78 °C (acetone/dry ice) and ammonia (150 mL) was added to this flask and condensed by ice. Lithium metal (58.34 mg, 8.32 mmol) was added to the flask and the solution was stirred for 1 h yielding a blue-black colored, stable dispersion. After the reaction fully finished, the cooling was removed and the solution was kept stirring until the complete evaporation of the ammonia. The resulting lithium-bronze was removed by a syringe and the DMSO solution was ultrasonicated for 30 min prior to the

addition of CO₂. All solution was transferred into an autoclave reactor which was subsequently sealed. CO₂ was purged to the reactor through a pressure valve (55 bar) keeping the stirring and constant pressure for 1 h. After reaction, the pressure was slowly released to atmospheric conditions. The resulting black solids were filtrated and dried in a vacuum oven at 75°C overnight.

2.4 Postfunctionalization of Zr⁴⁺@SWNT-(COOH) with Cyclo-(RGDfK) and Bombesin[7-13]

In a heat-dried and argon purged round-bottom flask (250 mL) equipped with two gas inlets and pressure compensation, Zr⁴⁺ filling and polycarboxylation functionalized SWNTs (Zr⁴⁺@SWNT-(COOH), 12 mg, 0.7 mmol of carbon) were dispersed in 100 mL THF by 30 min ultrasonication. Then the solution was cooled to 4°C in ice bath. EDC·HCl(N-(3-dimethylaminopropyl)-N'-ethylcarbodiimide hydrochloride) (201.3 mg, 1.05 mmol, 1.5 eq) and HOBt·H₂O(1-hydroxybenzotriazole hydrate)(141.9 mg, 1.05 mmol) was added sequentially to functionalized SWNTs solution and allowed to stir for 40 min in ice bath and to this solution was added Cyclo-(RGDfK) peptide (319.8 mg, 0.53 mmol, 0.75 eq) or Bombesin[7-13] (428.47 mg, 0.53 mmol, 0.75 eq). The pH value of solution was adjusted to 9 with DIPEA. Then the ice bath was removed and the solution was stirred at room temperature for 96 h. Afterwards the reaction was transferred to a separation funnel with cyclohexane and water (each 100 mL). The water/THF phase was discarded, and the cyclohexane layer with the functionalized nanotubes was purged two times with water and THF (100 mL, each). The organic layer with the functionalized nanotubes was filtered through a 0.2 μm reinforced cellulose membrane filter (Sartorius) and thoroughly washed with THF, ethanol, water and saturated aqueous Na₂CO₃ Solution, 200 mL each. The resulting solid was dried in a vacuum oven at 75°C overnight.

2.5 Characterization

TGA-MS was performed on a Perkin-Elmer Pyris 1 thermogravimetric analyzer equipped with a Hiden HPR20 mass spectrometer. The initial sample weights were about 1-3 mg, and the whole experiment was executed under inert gas atmosphere with a He gas flow(20 mL/min) at a ramp rate of 10 °C min⁻¹ to 700 °C after being held at 120 °C for 30 min to remove any residual solvent.

UV/Vis-NIR absorption spectra were recorded on a Perkin-Elmer Lambda 900 spectrometer. The samples were prepared by dispersing the nanotube material in H₂O by sonication in an ultrasonic bath (Ultrawave U50, 30-40 kHz) for 5 min followed by filtration through a plug of cotton wool to remove particulates after allowing the solution to stand for 2 h. The concentrations of SWNTs in the supernatant solutions were calculated with the extinction coefficient reported elsewhere.

Raman spectroscopy was performed using a Renishaw upright microscope using 830 nm for excitation, LWD objective 2 cm, operated at 50 × magnifications. Laser power magnification at the sample was 220 mW and spot size 100 micrometers. All spectra were recorded on solid samples over several regions and were referenced to the silicon line at 520 cm⁻¹.

High resolution transmission electron microscopy (HR TEM) images were taken on a high resolution microscope Jeol 3000F

coupled with EDX (point resolution, 0.16 nm) or a Jeol 4000F. Samples for HR TEM observation were ground and dispersed in ethanol and placed dropwise onto a holey carbon support grid.

ζ-Potential measurements were conducted on a Malvern Zetasizer NanoZS system with irradiation from a 632.8 nm He-Ne laser. The samples were filled in folded capillary cells and measured using a mixed mode method combining fast field reversal and slow field reversal, which eliminated electroosmotic effects. The ζ -potential was determined from the measured electrophoretic mobility (μ), using the Smoluchowski approximation:

$$\mu = \frac{\zeta \epsilon_m V}{4\pi\eta D}$$

where V is the applied voltage, η is the viscosity of the solution, ϵ_m is the dielectric constant of the medium, and D is the electrode separation. This approximation is rigorously valid only for spherical particles, and may overestimate in some cases the actual zeta potential²⁹⁻³¹. Nevertheless it has been successfully applied to nanotube dispersions to qualitatively understand the influence of the surface charge on dispersion quality³²⁻³⁵.

2.6 Concentration calibration and solubility determination of SWNT-(COOH)_n-peptide

A UV-vis-NIR absorption-based approach is used for a direct measurement of the unknown concentration of SWNT in aqueous supernatant via the Beer-Lambert law, according to the relation $A = \alpha cl$, where A is the absorbance, l [m] is the light path length, c [g/L] is the concentration of dispersed graphitic material, and α [Lg⁻¹m⁻¹] is the absorption coefficient. The stock SWNT solution was diluted to 10%, to avoid possible scattering losses at higher concentrations. For this purpose, peptide SWNT conjugates dispersions with different known concentrations ranging from 0.06 to 0.003 g/L are prepared for absorption measurements. The wavelength at 660 nm caused by the eh22 transition in the absorption spectra is chosen for determined for different SWNT concentrations.

2.7 Cell Culture and Receptor Binding (IC₅₀) Assays

The RGP receptor binding affinity (IC₅₀) of SWNT-(COOH)_n-Bombesin was determined by a competitive cell-binding assay on PC-3 cells in cultures using ¹²⁵I Tyr4-bombesin as the GRP-specific radioligand, while ¹²⁵I-echistatin was used as the integrin-specific radioligand for assessment of IC₅₀ of SWNT-(COOH)_n-RGDfK with integrin α_vβ₃ on human glioblastoma U87MG cells.

PC-3 cells were cultured at 37 °C in a humidified atmosphere of 5% CO₂ in air and split once confluence had been reached, using Dulbecco's modified Eagle medium (DMEM) medium with 10% fetal bovine serum (FBS), 200 U mL⁻¹ L-glutamine and 100 U mL⁻¹ penicillin. U87MG human glioblastoma cells were grown in Dulbecco's medium (Gibco) supplemented with 10% FBS, 200 U mL⁻¹ L-glutamine and 100 U mL⁻¹ penicillin.

During the cell-binding assay experiment, the human glioblastoma U87MG cells or PC-3 cells were harvested, washed twice with PBS, and resuspended (2 × 10⁶ cells/mL) in binding buffer (20 mmol/L Tris, pH 7.4, 150 mmol/L NaCl, 2 mmol/L CaCl₂, 1 mmol/L MgCl₂, 1 mmol/L MnCl₂, 0.1% bovine serum

albumin). 2×10^5 cells/mL U87MG cells were seeded in 96-well plates and incubated with ^{125}I -echistatin (30,000 cpm/well) in the presence of increasing concentrations of SWNT-(COOH)_n-RGDFK (0–100 $\mu\text{g/mL}$). For SWNT-(COOH)_n-Bombesin affinities test, 2×10^5 cells/mL PC-3 cells were incubated at 37 °C for 40 min under 5% CO₂ in the presence of 20,000 cpm ^{125}I -[Tyr⁴]Bombesin (2,200 Ci/mmol) and increasing concentration of SWNT-(COOH)_n-Bombesin conjugates (0–100 $\mu\text{g/mL}$). The total incubation volume was adjusted to 200 μL . After the cells were incubated for 2 h at room temperature, the medium was removed and washed twice with cold binding buffer. The radioactivity bound with cell was determined using a NaI(Tl) γ -counter (Packard Instruments). The 50% inhibitory concentration (IC₅₀) values for the U87MG cells were calculated by fitting the data by nonlinear regression using Origin 8.0 software. Experiments were performed twice with triplicate samples.

3. Results and discussion

The steam method was used to remove the catalyst encapsulated carbon anion, amorphous carbon layers, and opening of SWNTs following a method first reported by the research group of Professor Malcolm Green, University of Oxford with Thomas Swann Ltd. As-made SWNTs were purified by introducing steam carried by an argon flow through the reactor. This method gives rise to highly purified, opened CNTs, containing only SWNTs (when as samples are used) with dimensions ranging between 50–500 nm and diameters between 0.9 and 2 nm.

Although filling SWNTs with metal species is well established through the pioneering work of the Oxford Nanotube Group,^{14–16} the encapsulation of Zr⁴⁺ ions within SWNTs from aqueous solutions under rapid and mild conditions applicable for tracer preparation for PET radio-imaging has not been demonstrated. In this work, the Zr⁴⁺ filling experiment was performed from aqueous solutions using Zr(OAc)₄ as the precursor as a model for the PET radioisotope filling with ^{89}Zr .^{36–38} Gel formation occurred in the Zr(OAc)₄ solution until the pH value was adjusted to 2.4 by the dropwise addition of H₂SO₄ to the gelatinous sample. Subsequently, the successful zirconium filling was achieved. However, the precise nature of the encapsulated Zr clusters is difficult to predict due to the complex aqueous chemistry of Zr(IV). The Zr⁴⁺@SWNT structures were analyzed using High Resolution TEM (HRTEM). By lowering the accelerating voltage, the knock-on damage of the carbon nonmaterial can be minimized. From HRTEM observations, crystal-filled CNTs were only found in sample 1 (C₇₀@Zr⁴⁺@SWNT saturated with NaOAc, see experiments section), indicating that the solution saturated with OAc⁻ is a key factor in Zr filling (Figure 1a, b). Zirconium clusters were formed after the hydrolysis of precursor Zr(OAc)₄ in acetic acid and the condensation of partially hydrolyzed species after 48h is likely to form a three-dimensional

gel network. The zirconium complex structure is likely to change after addition of sulfuric acid at pH 2.4 as the stoichiometry of Zr(IV) to the oxo-ions in solution is known to be strongly dependent on the pH. It is likely that the sulfate SO₄²⁻ ions bind to Zr⁴⁺ and this counterion is expected to replace the AcO⁻ ions, but the precise nature of the zirconium clusters in this aqueous mixture could not be determined. Zirconium sulfate-based oxo-clusters are likely to be present in solution and may be introduced into the open-ended SWNTs by solution filling.^{39, 40} The filling experiment at low pH values seemed to help convert the zirconium-aqueous gel-like material into discrete species, which in turn contributed to the successful filling of the SWNTs with Zr(IV) by the solution method.

The use of functionalized C₆₀ was shown to allow the removal of the excess free salts in water.⁴¹ We found that the leaking of the encapsulated metallic species from open SWNTs may be prevented by the simultaneous encapsulation of C₇₀ molecules (maximum *van der Waals* radii *ca.* 1.1 nm) rather than C₆₀ (maximum external diameter = 0.7 nm), which remain stuck at the ends of the SWNTs. Several C₇₀ molecules act as ideal-sized stoppers for the SWNTs carriers. HRTEM images show that the open ends of SWNTs are filled by several C₇₀ molecules by standard endohedral encapsulation methods.⁴¹ We found that any free, un-bound C₇₀ decorating the outside of the tubes can be removed via washing with toluene followed by the filtration/dispersion. After fullerene encapsulation, the mixture containing M@C₇₀@SWNTs were then filtered and the solid residue was washed several times with distilled water to remove the Zr(IV) ions external to the SWNTs. Washing with water and toluene removed most of the free C₇₀ adhering to the walls of the SWNTs, in addition to any other of bulk materials from the filling step that were external to the SWNT cavity.

Raman spectroscopy studies showed that sample 1 and 2 (Sample 1: C₇₀@Zr⁴⁺@SWNTs saturated with NaOAc; Sample 2: C₇₀@Zr⁴⁺@SWNTs without NaOAc, see Material and Methods) exhibited characteristic radial breathing mode (RBM), G bands, and D bands (Figure 1d). For sample 1 and 2, the D-band intensities decreased with respect to those of purified SWNTs, indicating that functionalization occurred. The I_D/I_G ratio of purified SWNTs, sample 1, and sample 2 were 0.121, 0.076 and 0.046, respectively. Clearly, there is a decrease of the band intensity ratio after filling with zirconium.

The sidewall carboxylation of CNTs was achieved by a modified Birch reaction which was reported before⁴². This controllable and efficient carboxylation was based on the reduction of SWNTs in liquid ammonia to form the SWNT⁻ intermediates which act as electron donors, transferring one electron to the CO₂, yielding the respective carboxyl radical CO₂^{-•}. This radical species can subsequently attack the SWNT sidewall giving rise to carboxylated CO₂-SWNT derivatives (Figure 2a).

ARTICLE TYPE

Cite this: DOI: 10.1039/c0xx00000x

www.rsc.org/xxxxxx

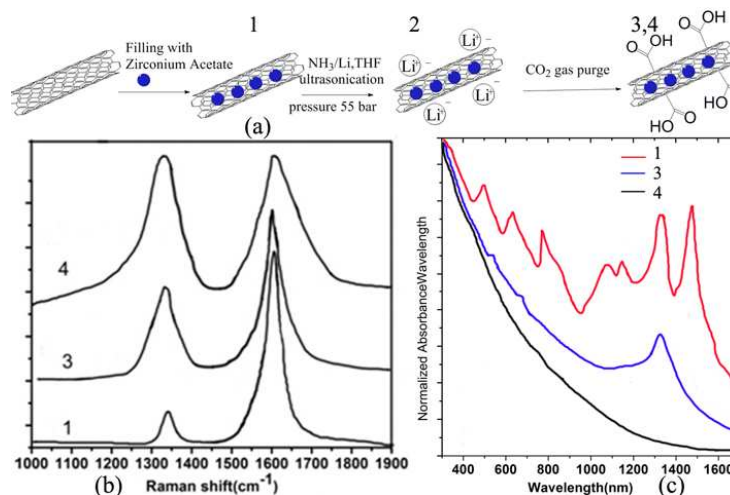


Figure 2. (a) Scheme of reductive polycarboxylation of Zirconium filled SWNTs under modified Birch conditions. (b) Raman D- and G-band region of sidewall carboxylated Zr⁴⁺@SWNT: Zr⁴⁺@SWNT-(COOH)_m (THF/ultrasound)(3), Zr⁴⁺@SWNT-(COOH)_n (THF/ultrasound/55bar) (4) compared with starting materials: Zr⁴⁺@SWNT(1). Excitation wavelength λ_{exc} = 830 nm. (c) UV-vis/nIR absorption spectra of starting material Zr⁴⁺@SWNT and carboxylated SWNT derivatives Zr⁴⁺@SWNT-(COOH)_m (THF/ultrasound) (3), Zr⁴⁺@SWNT-(COOH)_n (THF/ultrasound/55bar) (4) in DMF.

In this modified Birch reaction, the CNTs was dispersed via ultrasound in dry THF, and then the SWNTs were reduced with lithium metal in a liquid of ammonia condition. Afterwards, the ammonia was evaporated and remaining lithium-bronze can be removed forming a stable black solution with charged SWNTⁿ⁻ species. Prior to the carboxylation, an ultrasonication step is essential for efficiently debundle CNTs, which were then reduced to charged SWNTⁿ⁻ intermediates.

To this SWNTⁿ⁻ intermediate solution, gaseous carbon dioxide was purged to yield the respective polycarboxylated CO₂-SWNT derivatives after the final wash/workup. Raman spectroscopy method was explored for the study of polycarboxylation of SWNTs. The direct sidewall carboxylation of CNTs can induce a prominent Raman spectra change with an increased intensity of the D-band (~1300 cm⁻¹) based on the rehybridization of the sp² lattice carbon atoms into the sp³ configuration.

The resonant Raman spectra obtained with an excitation wavelength of 830 nm clearly showed a significant increase in the D-band intensity (Figure 2b) of sidewall functionalized SWNTs. The normalized area ratio of the D-band to the G-band (1590 cm⁻¹) (A_D/A_G) with respect to the ratio of the as-received starting material (A_{D0}/A_{G0}) can be regarded as a good measure for the degree of functionalization. The highest degree of sidewall functionalization was achieved when 50 bar pressure was applied (denoted as Zr⁴⁺@SWNT-(COOH)_n, n = 7.56 × 10⁵ [unit/CNT]), as compared to the Birch reduction without pressure. Specifically, the A_D/A_G ratio reached up to 20.2, while the A_D/A_G ratio of Zr⁴⁺@SWNT-(COOH) without pressure was only 6.3 (denoted as

Zr⁴⁺@SWNT-(COOH)_m, m = 9.34 × 10⁴). This indicated that the polycarboxylation of CNTs was highly dependent on the pressure applied in the reaction.

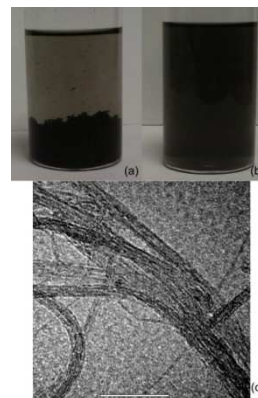
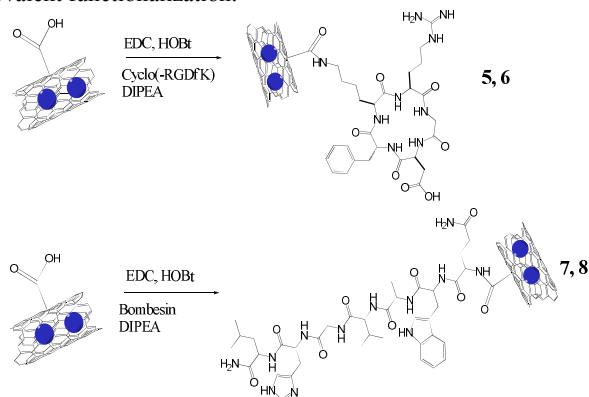


Figure 3. Photographs showing (a) the precipitate of starting materials: C₇₀@Zr⁴⁺@SWNTs (1) compared with (b) dissolution of Zr⁴⁺@SWNT-(COOH)_n (THF/ultrasound/55bar) (4) in DMF and (c) HR-TEM image of Zr⁴⁺@SWNT-(COOH)_n (THF/ultrasound/55bar) (4), scale bar 50 nm.

The UV-Vis-NIR absorption spectra were studied to reveal the excitonic transitions of SWNTs after functionalization. The spectrum of 1 showed resolved absorption signals for the metallic M11 transitions from (350-600 nm), as well as from the S22 (600-1000 nm) and S11 (1100-600 nm) transitions (Figure 2c). In contrast, the spectra of the functionalized SWNT derivatives only exhibited decreased metallic absorption signals in the M11 region between 500 and 600 nm. In the S22 and S11 regions,

there were no semiconducting absorption signals detectable. Two potential explanations can be attributed to the nearly complete absence of the characteristic SWNT transitions in highly functionalized $Zr^{4+}@SWNT-(COOH)_n$ (THF/ultrasound/55bar) (4). One is a lack of debundle and another is covalent modification of the nanotube network. The morphology of sample 4 in TEM images clarified this issue. Representative TEM image of sample 4 (Figure 3 c) shows that the nanotubes were well dispersed and individualized. The loss of the transitions in the absorption spectra was predominantly attributed to the covalent functionalization.



Scheme 1. EDC-mediated coupling of targeting peptides with Zirconium filled, carboxylated SWNTs yielding the corresponding products: $Zr^{4+}@SWNT-(COOH)_n-RGDfK$ (5), $Zr^{4+}@SWNT-(COOH)_m-RGDfK$ (6), $Zr^{4+}@SWNT-(COOH)_n-Bombesin$ (7) and $Zr^{4+}@SWNT-(COOH)_m-Bombesin$ (8).

The prominent benefit of polycarboxylation of CNTs is the formation of functionalized SWNTs with highly accessible surfaces which can be post-functionalized by adding other adducts via EDC coupling (scheme 1). Here, $Zr^{4+}@SWNT-(COOH)_x-RGDfK$ and $Zr^{4+}@SWNT-(COOH)_x-Bombesin$ ($x=n, m$) were successfully synthesized by coupling $Zr^{4+}@SWNT-(COOH)_x$ ($X=n, m$) to the amino group of Bombesin's glutamine residue or the amino group of RGDfK. The synthesis of highly dispersed $Zr^{4+}@SWNT-(COOH)_m$ (3) and $Zr^{4+}@SWNT-(COOH)_n$ (4) is a fundamental step for subsequent functionalization of RGDfK and Bombesin to the surface of $SWNT-(COOH)_x$ through EDC coupling. Composites $Zr^{4+}@SWNT-(COOH)_x-RGDfK$ and $Zr^{4+}@SWNT-(COOH)_x-Bombesin$ have good solubility in DMSO, H_2O and cell culture medium, which was necessary for the biomedical assessment.

The respective TGA trace in combination with the ion currents of the detected peptides (RGDfK, Bombesin) for the peptide coupled SWNT derivatives $Zr^{4+}@SWNT-(COOH)_n-RGDfK$ (5) and $Zr^{4+}@SWNT-(COOH)_n-Bombesin$ (7) are depicted in Figure 4. The major mass loss occurred in the temperature range between 300 and 500°C (35.3% mass loss for 5 and 32.3% mass loss for 7) and was accompanied by the detection of the $[RGDfK+H]^+$ ($m/z=604.4$) fragments as shown in Figure 4 (a), and $[Bombesin+H]^+$ ($m/z=809.4$), $[Bombesin/2 + H]^+$ ($m/z=405.38$) fragments in Figure 4 (b). Assuming that the difference in weight between the functionalized derivatives $Zr^{4+}@SWNT-(COOH)_n-RGDfK$ (5), $Zr^{4+}@SWNT-(COOH)_n-$

Bombesin (7) and the pristine starting material can be correlated with the weight of the detached functional entities and that the residual weight can be attributed to the defunctionalized SWCNTs, the loading amount of RGDfK and Bombesin on the SWNT can be calculated. It revealed the presence of ~1 RGDfK molecule for every 92 (1.09 atomic %) carbon atoms for $Zr^{4+}@SWNT-(COOH)_n-RGDfK$ (5), ~1 Bombesin molecule for every 141 (0.71 atomic %) carbon atoms for $Zr^{4+}@SWNT-(COOH)_n-Bombesin$ (7).

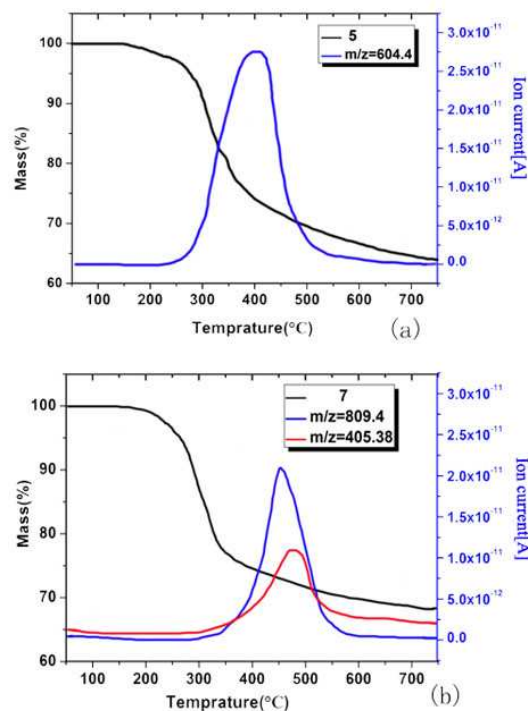


Figure 4. (a) Thermogravimetric profile (weight loss, black) of TGA-MS for $Zr^{4+}@SWNT-(COOH)_n-RGDfK$ (5) (heating rate: 10°C/min), and the detected ion currents for the RGDfK fragments $m/z = 604.4$ ($[M+H]^+$) (blue). (b) Thermogravimetric profile (weight loss) of $Zr^{4+}@SWNT-(COOH)_n-Bombesin$ (7) (heating rate: 10K/min), vertical arrow corresponds to the weight loss (black) recorded within the temperature region of Bombesin peptide fragment detection (300-500°C) - in combination of the detected ion currents for the two different potential Bombesin fragments $m/z = 809.4$ (blue), $m/z = 405.38$ (red) (corresponding to $[M]^{2+}$ and $[M]^+$)

It is important to investigate the solubility and dispersibility of peptide SWNT conjugates in aqueous media before we can move forward to biomedical experiment or application. To avoid unwanted precipitate of the SWNTs in solution, samples were mildly centrifuged (3 krpm, 5 min) after the wet chemical processing and the functionalization to remove the aggregate. SWNT concentrations (c) absorption calibration curves for $SWNT-(COOH)_n-Bombesin$ and $SWNT-(COOH)_n-RGDfK$ are shown in Figure 5b. The slope of the curves gives the values of C value at wavelength of 660nm. In this study the extinction coefficient corresponding to the eh22 transition (660nm) is 3500 $Lg^{-1}m^{-1}$ for the $SWNT-(COOH)_n-peptide$ dispersions.

The solubility and dispersibility data show that the dispersion efficiency in of $Zr^{4+}@SWNT-(COOH)_n-RGDfK$ 5 and $Zr^{4+}@SWNT-(COOH)_n-Bombesin$ 7 could reach 89% and 87%

respectively after covalent attachment of the carboxylic acid groups and functionalized with peptides (Table 1). This data indicated that these functionalized SWNTs are highly soluble in aqueous media.

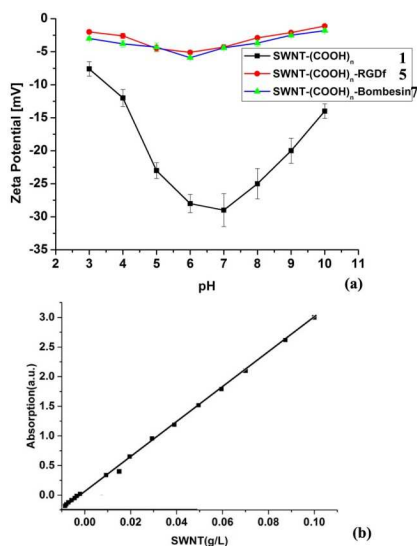


Figure 5. (a) Plot of the zeta potential of functionalized SWNTs as a function of the pH value. (b) Absorption calibration curves for SWNT obtained by monitoring the eh22 transition at wavelength of 660nm.

Figure 5a records the zeta potential of SWNT-(COOH)_n, SWNT-(COOH)_n-RGDfK and SWNT-(COOH)_n-Bombesin as a function of the pH value. Aqueous suspensions of SWNT-(COOH)_n, SWNT-(COOH)_n-RGDfK and SWNT-(COOH)_n-Bombesin are robust at pH conditions ranging from 3 to 10 without any observed precipitate. The zeta potential of SWNT-(COOH)_n becomes more negative with increasing pH until a neutral pH 6-7 is reached and then starts to increase again. The increase in the magnitude of the zeta potential with pH increasing from 3 to 7 can be explained by the ionization of the COOH groups on the SWNT. The peptide covalent functionalization has a dramatical influence in the reduction of the zeta potential of SWNT-(COOH)_n, the zeta potential is shifted to a value range from 0 to -5 mV.

Table 1. Dispersability and receptor binding affinity of SWNT-COOH-peptide nano-constructs

Sample	5	6	7	8
Dispersability (H ₂ O)	89%	13%	85%	9%
Solubility (g/L)	0.025 ± 0.001	0.013 ± 0.003	0.031 ± 0.003	0.011 ± 0.002
IC ₅₀ (μg/mL)	4.21 ± 0.86	22.62 ± 3.97	5.80 ± 0.54	16.70 ± 2.24

The dispersibility is directly deduced from the ratio of the initial SWCNT concentrations 0.1 g L⁻¹ to the actual concentrations in the supernatant.

Before the binding affinity study of peptide SWNT conjugates, we evaluated the cytotoxicity of these multifunctional SWNTs to ensure the materials' concentration used for the next binding assay is safe to cells. Based on the studies of SWNT's cytotoxicity from literature⁴³⁻⁴⁶, PC-3 cells were treated with 5 μg/ml to 800 μ

g/ml of SWNT-(COOH)_n and SWNT-(COOH)_n-Bombesin for 24 h, glioblastoma U87MG cells were treated with 5 μg/ml to 800 μg/ml of SWNT-(COOH)_n and SWNT-(COOH)_n-RGDfK for 24 h, respectively. The effect of three types of SWCNTs on cell viability was evaluated by MTT assay. As shown in Figure 6, treatment of the U87MG cells and PC-3 cells with SWNT-(COOH)_n decreased cell viability in a time and dose-dependent manner. The results showed that the EC₅₀ values of was 454.1 ± 9.8 when PC-3 cells were treated with SWNT-(COOH)_n for 24 h, and 454.1 ± 9.8 when U87MG cells were treated with SWNT-(COOH)_n for 24 h. For SWNT-(COOH)_n-RGDfK and SWNT-(COOH)_n-Bombesin, both have maximum of 37.0% (in U87MG cells) and 34.6% (in PC-3 cells) inhibition at 800 μg/ml SWNT in comparison to the control. Therefore, no EC₅₀ values can be determined from the MTT assay for both peptide functionalized SWNTs, as maximum cytotoxicity determined in both instances was less than 50%. Results from the MTT assay indicated the Bombesin or RGDfK functionalized SWNT to have very low acute toxicity to the PC-3 cells and U87MG cells respectively, as the 24 h EC₅₀ values exceeded the limited concentration we can use (800 μg/ml).

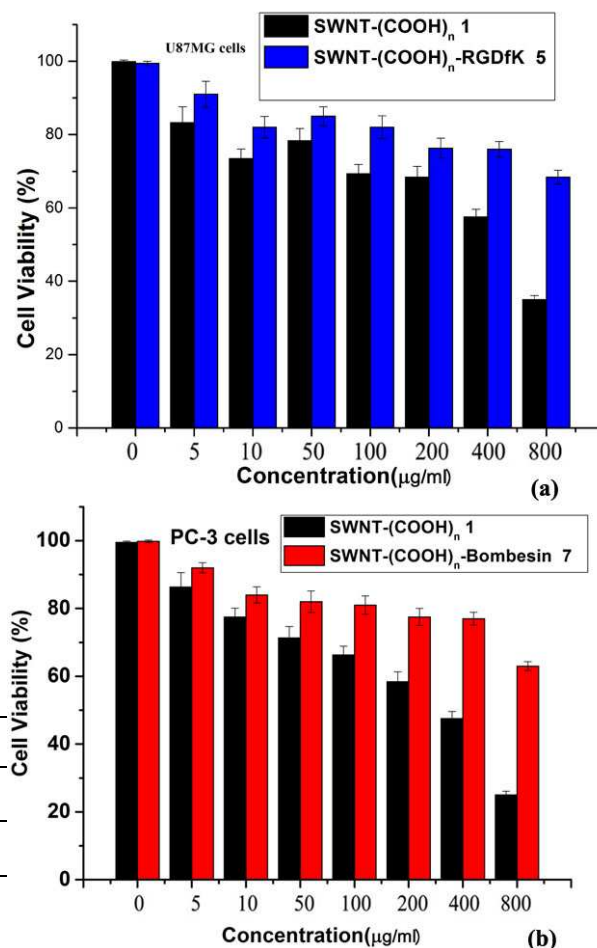


Figure 6. (a) Effect of SWNT-(COOH)_n 1, SWNT-(COOH)_n-RGDfK 5 on cell viability of U87MG cells, and (b) Effect of SWNT-(COOH)_n 1, SWNT-(COOH)_n-Bombesin 7 on cell viability of PC-3 cells. Cells were treated with SWNTs for 24 h at 37 °C. Cell viability was measured by the MTT method as described in materials and methods. Data are shown as mean ± SD values obtained from three separate experiments.

The binding affinities (IC_{50}) of SWNT-COOH-Peptides conjugates have been evaluated by competitively displacing radio-iodinated Bombesin ^{125}I -[Tyr⁴]BBN by adding increasing amounts of SWNT-(COOH)_m-Bombesin to the surface of PC-3 cells, and displacing the integrin-specific radioligand ^{125}I -echistatin with the SWNT-(COOH)_n-RGDfK conjugate from human glioblastoma U87MG cells. Plots of cell-bound radioactive peptides (Bombesin or RGDfK) versus increasing concentrations of SWNT-COOH-peptide conjugates have been used to determine IC_{50} values. It is evident from the data that the IC_{50} values or cell binding affinities of the conjugates depends on the degree of carboxylation on the CNT surface. Applying a high pressure (55 bar) during the reaction leads to a dramatic increase in the number of carboxyl groups covalently attached to the CNT surface. The functionalized CNTs used for EDC coupling with peptides can naturally load more bombesin/RGDfK peptides on the surface and exhibit a lower IC_{50} value (or a higher cell binding affinity) when compared with functionalized CNT synthesized without pressure (Table 1).

4. Conclusion

We demonstrated an aqueous solution method filling of SWNTs with Zr^{4+} by adjusting the pH to ca. 2 with H_2SO_4 . Any significant leakage of metal ions from open SWNTs was avoided by simultaneous encapsulation of C_{70} molecules at the ends of SWNTs. The successful inner cavity filling with Zr^{4+} and both ends stacking with C_{70} molecules were imaged by HRTEM in this solution filling method. Then we explored the polycarboxylation of SWNTs by the reductive treatment of the tubes in sodium metal-ammonia solutions followed by use of gaseous carbon dioxide as electrophilic trapping molecules. Moreover, the initially introduced carboxylic acid functionalities served as anchoring points for subsequent coupling with peptides via an EDC-mediated reaction. The successful addition of specific peptides on SWNTS-(COOH)_x was confirmed by the TGA-MS-based analysis of the functionalized SWNT derivatives. For both attached addends, the corresponding characteristic molecule fragments can be detected in the temperature region of a covalent bond cleavage. The solubility of functional SWNTs was precisely measured and confirms that both SWNT-peptide conjugates show excellent dispersibility in aqueous condition. The surface charge measurement reveals that the zeta potential of peptide covalent functionalized SWNTs shift to neutral compared to the higher negatively charged SWNT-(COOH)_n, which is much more benefit for the cells' internalization and membrane transportation of SWNTs. The binding assay shows that higher carboxylated SWNT-COOH-peptides could load more addends on the surface and exhibited a lower IC_{50} value upon binding to PC-3 cells. The investigation of these polycarboxylated SWNT-COOH-peptides opens a new chapter for the application of carbon nanotube as targeting delivery therapy agent.

Notes and references

¹ State key Laboratory of Heavy Oil Processing, China University of Petroleum, Beijing 102249, China

²Department of Applied Chemistry, China University of Petroleum, Beijing 102249, China, E-mail: zh209@cup.edu.cn

† Electronic Supplementary Information (ESI) available: [Steaming purification of SWNTs; Synthesis of bombesin [7-13] peptide (2) and cyclic deprotected RGDfK peptide; ¹HNMR]. See DOI: 10.1039/b000000x/

‡ Footnotes should appear here. These might include comments relevant to but not central to the matter under discussion, limited experimental and spectral data, and crystallographic data.

References

1. S. Iijima, *Nature*, 1991, **354**, 56.
2. A. M. Diez-Pascual and D. Gascon, *ACS Appl Mater Inter*, 2013, **5**, 12107.
3. Y. S. Park, J. Yi and J. Lee, *Thin Solid Films*, 2013, **546**, 81.
4. S. Beg, M. Rizwan, A. M. Sheikh, et al., *J Pharm Pharmacol*, 2011, **63**, 141.
5. X. Li, Y. Fan and F. Watari, *Biomed Mater*, 2010, **5**.
6. F. Liang and B. Chen, *Curr Med Chem*, 2010, **17**, 10.
7. H.-C. Wu, X. Chang, L. Liu, et al., *J Mater Chem*, 2010, **20**, 1036.
8. A. Ghosh, K. V. Rao, R. Voggu, et al., *Chem Phys Lett*, 2010, **488**, 198.
9. Z. Yang, Z. Wang, X. Tian, et al., *J Chem Phys*, 2012, **136**.
10. B. Gebhardt, F. Hof, C. Backes, et al., *J Am Chem Soc*, 2011, **133**, 19459.
11. B. Gebhardt, Z. Syrgiannis, C. Backes, et al., *J Am Chem Soc*, 2011, **133**, 7985.
12. D. Wunderlich, F. Hauke and A. Hirsch, *J Mater Chem*, 2008, **18**, 1493.
13. J. Chattopadhyay, A. K. Sadana, F. Liang, et al., *Org Lett*, 2005, **7**, 4067.
14. J. L. Hutchison, J. Sloan, A. I. Kirkland, et al., *J Electron Microsc (Tokyo)*, 2004, **53**, 101.
15. C. G. Xu, J. Sloan, G. Brown, et al., *Chem Commun*, 2000, 2427.
16. R. R. Meyer, J. Sloan, R. E. Dunin-Borkowski, et al., *Science*, 2000, **289**, 1324.
17. M. Wilson and P. A. Madden, *J Am Chem Soc*, 2001, **123**, 2101.
18. G. Brown, S. R. Bailey, J. Sloan, et al., *Chem Commun*, 2001, 845.
19. N. Thamavaranukup, H. A. Hoppe, L. Ruiz-Gonzalez, et al., *Chem Commun*, 2004, 1686.
20. P. Chowdhury, M. Gondry, R. Genet, et al., *Photochem Photobiol*, 2003, **77**, 151.
21. S. J. Miller, B. P. Joshi, Y. Feng, et al., *Gastroenterology*, 2011, **140**, S104.
22. H. Sahoo and W. M. Nau, *Chembiochem*, 2007, **8**, 567.
23. S. Scheffler, M. Sauer and H. Neuweiler, *Z Phys Chem*, 2005, **219**, 665.
24. L. Voglino, S. A. Simon and T. J. McIntosh, *Biochemistry-us*, 1999, **38**, 7509.
25. X. Wen, C. Chao, K. Ives, et al., *BMC Mol Biol*, 2011, **12**.
26. M. A. Dechantsreiter, E. Planker, B. Matha, et al., *J Med Chem*, 1999, **42**, 3033.
27. R. Haubner, H. J. Wester, W. A. Weber, et al., *Cancer Res*, 2001, **61**, 1781.
28. U. Hersel, C. Dahmen and H. Kessler, *Biomaterials*, 2003, **24**, 4385.

29. A. A. Ameen, A. N. Giordano, J. R. Alston, et al., *Phys Chem Chem Phys*, 2014, **16**, 5855.
30. H. Journal Of Physical Chemistry BKato, A. Nakamura and M. Horie, *RSC Adv*, 2014, **4**, 2129.
- 5 31. R. W. O'Brien, J. K. Beattie and A. M. Djerdjev, *J Colloid Interf Sci*, 2014, **420**, 70.
32. K. Min, J. Kim, K. Park, et al., *J Mol Catal B-enzym*, 2012, **83**, 87.
33. Z. Sun, V. Nicolosi, D. Rickard, et al., *J Phys Chem C*, 2008, **112**, 10692.
- 10 34. E. F. de la Cruz, Y. Zheng, E. Torres, et al., *Int J Electrochem Sc*, 2012, **7**, 3577.
35. B. White, S. Banerjee, S. O'Brien, et al., *J Phys Chem C*, 2007, **111**, 13684.
36. Y. Zhang, H. Hong and W. Cai, *Curr Radiopharm*, 2011, **4**, 131.
- 15 37. M. A. Deri, S. Ponnala, B. M. Zeglis, et al., *J Med Chem*, 2014, **57**, 4849.
38. A. Kasbollah, P. Eu, S. Cowell, et al., *J Nucl Med Technol*, 2013, **41**, 35.
39. A. C. Geiculescu and H. J. Rack, *J Non-cryst Solids*, 2001, **289**, 53.
- 20 40. A. C. Geiculescu and H. J. Rack, *J Non-cryst Solids*, 2002, **306**, 30.
41. M. Yudasaka, K. Ajima, K. Suenaga, et al., *Chem Phys Lett*, 2003, **380**, 42.
42. B. Gebhardt, F. Hof, C. Backes, et al., *J Am Chem Soc*, 2011, **133**, 19459.
- 25 43. L. M. Pasquini, S. M. Hashmi, T. J. Sommer, et al., *Environ Sci Technol*, 2012, **46**, 6297.
44. R. Subbiah, S. Ramasundaram, P. Du, et al., *J R Soc Interface*, 2013, **10**, 20130694.
45. H. N. Yehia, R. K. Draper, C. Mikoryak, et al., *J Nanobiotechnology*, 2007, **5**, 8.
- 30 46. B. Farshid, G. Lalwani and B. Sitharaman, *J Biomed Mater Res A*, 2014.